Journal of the Korean Astronomical Society
52: 57 ∼ 69, 2019 June
https://doi.org/10.5303/JKAS.2019.52.3.57
pISSN: 1225-4614 · eISSN: 2288-890X
http://jkas.kas.org

Origin and Status of Low-Mass Candidate Hypervelocity Stars

Bum-Suk Yeom[1,2], Young Sun Lee[1], Jae-Rim Koo[1], Timothy C. Beers[3], and Young Kwang Kim[1]

[1]Department of Astronomy and Space Science, Chungnam National University, Daejeon 34134, Korea youngsun@cnu.ac.kr
[2]Jeollabukdo Institute of Science Education, Iksan 54549, Korea
[3]Department of Physics and JINA Center for the Evolution of the Elements, University of Notre Dame, IN 46556, USA

Received March 26, 2019; accepted May 17, 2019

Abstract: We present an analysis of the chemical abundances and kinematics of six low-mass dwarf stars, previously claimed to be candidate hypervelocity stars (HVSs). We obtained moderate-resolution ($R \sim 6000$) spectra of these stars to estimate the abundances of several chemical elements (Mg, Si, Ca, Ti, Cr, Fe, and Ni), and derived their space velocities and orbital parameters using proper motions from the *Gaia* Data Release 2. All six stars are shown to be bound to the Milky Way, and in fact are not even considered high-velocity stars with respect to the Galactic rest frame. Nevertheless, we attempt to characterize their parent Galactic stellar components by simultaneously comparing their element abundance patterns and orbital parameters with those expected from various Galactic stellar components. We find that two of our program stars are typical disk stars. For four stars, even though their kinematic probabilistic membership assignment suggests membership in the Galactic disk, based on their distinct orbital properties and chemical characteristics, we cannot rule out exotic origins as follows. Two stars may be runaway stars from the Galactic disk. One star has possibly been accreted from a disrupted dwarf galaxy or dynamically heated from a birthplace in the Galactic bulge. The last object may be either a runaway disk star or has been dynamically heated. Spectroscopic follow-up observations with higher resolution for these curious objects will provide a better understanding of their origin.

Key words: methods: data analysis — techniques: spectroscopic — Galaxy: disk — stars: abundances

1. Introduction

Hypervelocity stars (HVSs) are unbound and rare fast-moving objects in the Galactic halo, possessing space velocities that exceed the Galactic escape speed. The first HVS was discovered from a radial velocity survey of faint blue horizontal branch stars (Brown et al. 2005). It is a 3 $M_{\odot}$ main-sequence B-type star moving with a Galactic rest-frame velocity of about 700 km s^{-1} at a distance of about 100 kpc. Since then, about 20 B-type HVS candidates have been discovered in the Galactic halo (Brown et al. 2015). These intriguing objects are believed to originate from the so-called "Hills mechanism", which is associated with the supermassive black hole (SMBH) at the Galactic Center. This model suggests that the SMBH can disrupt close-by binary stars and eject one of the stars at speeds up to $\sim$ 1000 km s^{-1} (Hills 1988; Yu & Tremaine 2003). It is known that this mechanism can also produce HVSs bound to the Milky Way (MW) (Bromley et al. 2009; Brown et al. 2014).

In addition to the HVSs, there are fast-moving O and B type stars referred to as "runaway stars" which have peculiar velocities larger than 40 km s^{-1} (e.g., Gies 1987; Stone 1991; Tetzlaff et al. 2011). Several scenarios have been proposed to explain the runaway stars. The binary ejection mechanism (Blaauw 1961; Tauris & Takens 1998; Tauris 2015) postulates that these objects could be formed in binary systems in the Galactic disk and "released" by the explosive deaths of their companions. The dynamical ejection mechanism proposed by Poveda et al. (1967) assumes that a star can be ejected by multi-body interactions in a high-density environment such as a star cluster. Another explanation to account for these stars is ejection from a star-forming galaxy such as the Large Magellanic Cloud (LMC) (Boubert & Evans 2016). An alternative theory suggests that these objects are the members of a tidally disrupted dwarf galaxy (Abadi et al. 2009). Even though there exist many scenarios to explain the HVSs and runaway stars, full understanding of their origin remains elusive.

In spite of the ambiguity of their origin, high-velocity stars have received attention because they can provide a means for measuring the local escape velocity at a given distance from the Galactic Center, which can in turn constrain the total mass of the MW which is still uncertain by a factor of more than two (Xue et al. 2008; Watkins et al. 2010). We can utilize the general characteristics of HVSs to infer where they originated. What HVSs have in common is that they are young, massive main-sequence stars typically found at present distances beyond 50 kpc from the Sun (See Brown 2015, and references therein). Therefore, we can hypothesize that the high-velocity stars may originate from star-forming regions in the disk, bulge, or dwarf satellites of the MW.

Although most of the currently known HVSs and runaway stars are early type (high-mass) main-sequence stars, one might expect that the proposed ejection

Corresponding author: Y. S. Lee

Table 1
Details of spectroscopic observations

Object	Magnitude	Date (UT)	Exposure Time (s)	N_{obs}	S/N	Pal14 ID
PROGRAM STARS:	r_0					
J113102.87+665751.1	16.15	2014.01.05/12	3600	5	49	4
J064337.13+291410.0	18.01	2014.03.25	3600	3	30	7
J172630.60+075544.0	18.46	2014.05.03	3600, 4500	3	30	10
J095816.39+005224.4	17.51	2014.01.12	3600	3	40	15
J074728.84+185520.4	17.81	2014.03.25/30	4500, 4000	2	29	16
J064257.02+371604.2	16.87	2014.03.30	3600	3	37	17
STANDARD STARS:	V					
HIP 33582	9.01	2014.01.05	1, 4, 8, 30	4		
HIP 59330	8.59	2014.01.05	1, 3, 10, 15	4		
HIP 44075	5.86	2014.01.12	1, 2, 3, 5	4		
HIP 60551	8.00	2014.01.12	2, 3, 5, 10	4		
HIP 64426	7.29	2014.01.12	1, 2, 3, 5	4		
HR 2721	5.58	2014.03.25	1, 2, 5	3		
HR 2233	5.65	2014.03.30	1, 1, 1, 1, 5	5		
HIP 62882	8.38	2014.05.03	1, 3, 5, 10, 20	6		

N_{obs} is the number of observations. Pal14 ID is the ID of a star used in Pal14. r_0 indicates the reddening-corrected r magnitude. S/N is the signal-to-noise ratio of the co-added spectrum of each star after data reduction. The S/N range of the standard stars can be seen in Figure 3.

mechanisms could work for any stellar type, leading to the prospect of identifying low-mass HVSs (Kollmeier & Gould 2007). For this reason, various efforts to search for such stars have been carried out from the stellar database constructed by large spectroscopic surveys such as Sloan Digital Sky Survey (SDSS; York et al. 2000) and Large Sky Area Multi-Object Fibre Spectroscopic Telescope (LAMOST; Cui et al. 2012).

Indeed, Kollmeier et al. (2009) and Li et al. (2012) identified 6 and 13 HVS candidates, respectively, from SDSS. In addition, Zhong et al. (2014) reported 28 HVS candidates, 17 of which are F-, G-, and K-type dwarf stars. Li et al. (2015) reported another 19 low-mass HVS candidates from LAMOST. Palladino et al. (2014, hereafter Pal14) also reported the discovery of 20 low-mass G-, and K-type HVS candidates from Sloan Extension for Galactic Understanding and Exploration (SEGUE; Yanny et al. 2009). One interesting aspect of many of these low-mass candidates is that they appeared to be associated with birth in the Galactic disk, rather than the Galactic Center, as is the case for the high-mass HVSs.

Previous studies of low-mass HVSs or runaway star candidates were carried out exclusively on the basis of derived stellar kinematics, since proper motion information, when combined with an observed radial velocity and distance estimate, provides the full space velocity of a star. In keeping with this, it is interesting to note that HVSs thought to have a Galactic Center origin (e.g., the high-mass HVSs) are often well-separated in their proper motions from likely disk origins, which is not the case for the low-mass runaway-star candidates. For this reason, one might consider use of their detailed chemical-abundance patterns in order to identify the possible birthplaces of the runaway-star candidates – bulge, disk, or halo, and thereby constrain the possible ejection mechanisms of such stars.

We note here that a number of recent studies claim that most of the low-mass HVS candidates and runaway stars identified thus far are bound to the MW. For example, Ziegerer et al. (2015) have re-calculated the proper motions for the 14 HVS candidates that Pal14 reported, using images from SDSS,[1] Digitized Sky Survey[2] (DSS), and UKIDSS[3] (Lawrence et al. 2007). They found that the newly measured proper motions are much smaller than the ones used by Pal14, and, as a result, all of their HVS candidates are bound to the MW under three different potentials for the MW. More recently, Boubert et al. (2018) reported using *Gaia* Data Release 2 (DR2; Gaia Collaboration et al. 2018) proper motions and radial velocities that all late-type stars, which have been claimed to be HVSs previously are likely to be bound to the MW, except one object (LAMOST J115209.12+120258.0).

Prior to clarification on the proper motions for low-mass HVS candidates in the Pal14 sample, we carried out follow-up spectroscopic observations and obtained medium-resolution ($R = 6000$) spectra for six of them, in order to study their chemical abundance patterns. As we report in this paper, we make use of *chemical tagging* (Freeman & Bland-Hawthorn 2002), in an attempt to understand their characteristics and likely parent populations of their birthplaces. This approach has already proven to be useful to constrain the origin of HVSs or runaway stars (Hawkins & Wyse 2018). In addition, we make use of the greatly improved proper motion information from *Gaia* DR2 to carry out a kinematics anal-

[1] http://skyserver.sdss3.org/public/en/tools/chart/navi.aspx
[2] http://archive.stsci.edu/cgi-bin/dss_plate_finder
[3] http://www.ukidss.org/

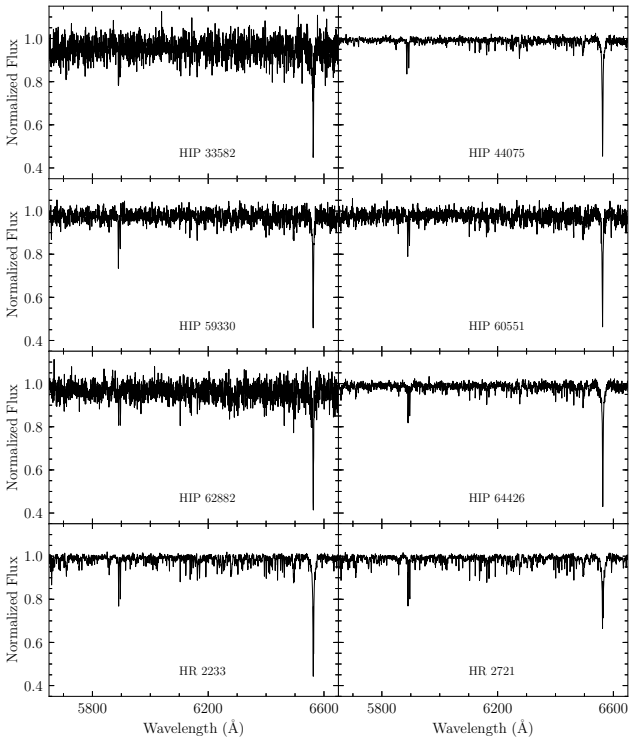

Figure 1. Spectra of standard stars in the wavelength range used to derive stellar parameters and chemical abundances.

ysis of our program objects. Although we confirm that none of our program stars is unbound, and thus none of them is a viable HVS candidate any longer, for simplicity we refer to them as HVS candidates through this paper. This paper is organized as follows. The spectroscopic observations and reduction of the six low-mass candidate HVSs are described in Section 2. In Section 3, we determine the stellar parameters and chemical abundances for our program stars. In Section 4, we present results of the analysis of the chemical and kinematic properties of our objects. Section 5 discusses the characteristics and possible origin of each HVS candidate. A summary of our results, and brief conclusions are provided in Section 6.

2. SPECTROSCOPIC OBSERVATIONS AND REDUCTION

Among the 20 HVS candidates reported by Pal14, we obtained spectroscopy for six stars during the period between January and May, 2014, including two stars that were not studied by Ziegerer et al. (2015). The spectra were obtained with the Dual Imaging Spectrograph (DIS) on the Apache Point Observatory 3.5 m telescope in New Mexico. We selected the grating combination B1200/R1200, which has wavelength coverage of 4200 – 5400 Å and 5600 – 6700 Å in the blue and red channels, respectively, along with a 1.5 arcsec slit, a yielding spectral resolving power of $R = 6000$, sufficient to perform a chemical abundance analysis for individual α-elements (Mg, Ca, Si, and Ti) and iron-group elements (Cr, Fe, and Ni).

In addition, we observed eight well-studied disk

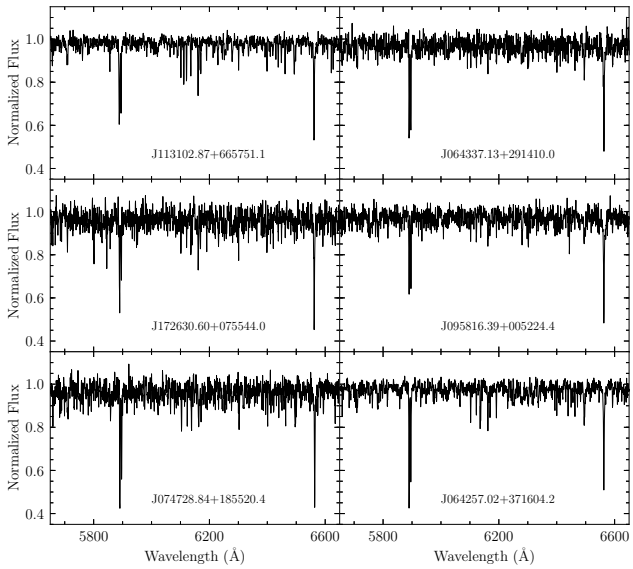

Figure 2. Same as in Figure 1, but for our program stars.

stars as comparison stars, to verify the accuracy of our derived stellar parameters ($T_{\rm eff}$, log g, and [Fe/H]) and chemical abundances for our program stars. For the comparison stars, we took several exposures to obtain the spectra at various signal-to-noise (S/N) ratios, enabling an evaluation of the effect of S/N on the estimated stellar parameters and chemical abundances of our target stars. As our targets are mostly faint ($r_0 > 16.0$), we took one or two exposures between 60 and 75 minutes each. Table 1 lists details of the observations.

We followed the standard spectroscopic reduction steps such as aperture extraction, wavelength calibration, and continuum normalization using IRAF.[4] Radial velocities were measured by cross-correlation of observed and theoretical template spectra using the `xcsao` task of the `rvsao` package (Kurtz & Mink 1998) in IRAF. In that process, we used a synthetic model spectrum of $T_{\rm eff} = 6000$ K and log $g = 4.0$ as a template. We also considered the night-sky emission lines to check for any additional instrumental shifts. The spectra of each star were co-added, after application of radial velocity corrections, to obtain a final spectrum with higher S/N, typically S/N $\sim 30 - 50$. The spectra of our standard stars and program stars are shown in Figures 1 and 2, respectively.

3. ESTIMATION OF STELLAR PARAMETERS AND CHEMICAL ABUNDANCES

We derived estimates of the values of stellar parameters ($T_{\rm eff}$, log g, and [Fe/H]), and elemental abundances for Mg, Si, Ca, Ti, Cr, and Ni using the Stellar Parameters And chemical abundances estimator (`SP_Ace`; Boeche & Grebel 2016) code. The `SP_Ace` code employs similar methodology to that used in the RAdial Velocity

[4] IRAF is distributed by the National Optical Astronomy Observatory, which is operated by the Association of Universities for Research in Astronomy, Inc., under cooperative agreement with the National Science Foundation.

Table 2
Stellar parameters and chemical abundances of the comparison stars adopted from the literature

Star	$T_{\rm eff}$ (K)	log g	[Fe/H]	[Mg/H]	[Si/H]	[Ca/H]	[Ti/H]	[Cr/H]	[Ni/H]	References
HIP 33582	5782	4.30	–0.68	–0.23	–0.36	–0.50	–0.33	–0.64	···	1, 3, 6, 8, 10
HIP 44075	5880	4.10	–0.90	–0.53	–0.55	–0.60	–0.57	–0.89	–0.87	1, 2, 3, 4, 5, 7, 11
HIP 59330	5749	4.02	–0.75	–0.45	–0.42	–0.58	–0.47	–0.74	–0.75	1, 3, 4
HIP 60551	5724	4.38	–0.86	–0.53	–0.52	–0.61	–0.59	–0.85	–0.76	1, 3, 4
HIP 62882	5692	3.81	–1.26	–0.73	–0.79	–0.93	–0.99	–1.30	–1.21	1, 3, 5, 11
HIP 64426	5892	4.19	–0.76	–0.39	–0.50	–0.62	–0.58	–0.81	–0.77	1, 3, 4, 8
HR 2233	6240	3.97	–0.19	–0.06	–0.11	–0.11	0.11	–0.22	–0.22	4, 5, 6, 7, 11
HR 2721	5872	4.30	–0.32	–0.13	–0.21	–0.25	–0.17	–0.35	–0.33	4, 5, 7, 9, 11

The numbers in the last column indicate the following references: (1) Bensby et al. (2003), (2) Bensby et al. (2005), (3) Fulbright (2000), (4) Lee et al. (2011), (5) Prugniel et al. (2011), (6) Houk & Swift (2000), (7) Takeda & Honda (2005), (8) Battistini & Bensby (2015), (9) Mishenina et al. (2013), (10) Delgado et al. (2014), (11) Cenarro et al. (2007). Where possible, we adopted the average of parameter and abundance values found in the literature.

Table 3
Stellar parameters and chemical abundances derived for our program stars

SDSS ID	Pal14 ID	$T_{\rm eff}$ (K)	log g	[Fe/H]	[Mg/Fe]	[Si/Fe]	[Ca/Fe]	[Ti/Fe]	[Cr/Fe]	[Ni/Fe]	[α/Fe]
J113102.87+665751.1	4	5038±235	4.47±0.41	–0.49±0.13	0.48	0.34	0.32	0.37	–0.07	–0.11	0.38
J064337.13+291410.0	7	5136±260	4.55±0.48	–0.60±0.14	0.47	0.21	–0.20	0.41	···	0.09	0.22
J172630.60+075544.0	10	4986±404	4.77±0.66	–0.69±0.16	–0.34	0.40	0.05	0.50	···	0.21	0.15
J095816.39+005224.4	15	5290±290	4.46±0.50	–0.55±0.15	–0.13	0.06	0.10	–0.22	0.62	–0.10	–0.05
J074728.84+185520.4	16	5446±282	4.10±0.50	0.27±0.14	–0.10	–0.20	–0.11	–0.41	–0.10	–0.06	–0.20
J064257.02+371604.2	17	5261±248	4.45±0.42	–0.12±0.13	0.05	–0.08	0.05	–0.09	0.18	0.14	–0.02

Note that the systematic offsets are corrected for these values. [α/Fe] is a mean value of [Mg/Fe], [Si/Fe], [Ca/Fe], and [Ti/Fe]. Typical errors for elements are σ[Mg/Fe] = 0.27 dex, σ[Si/Fe] = 0.17 dex, σ[Ca/Fe] = 0.15 dex, σ[Ti/Fe] = 0.18 dex, σ[Cr/Fe] = 0.20 dex, and σ[Ni/Fe] = 0.18 dex, respectively.

Experiment (RAVE; Steinmetz et al. 2006) chemical abundance pipeline (Boeche et al. 2011), which was developed to derive elemental abundances for the stellar spectra obtained by the RAVE survey. `SP_Ace` estimates the stellar parameters and abundances based on a library of equivalent widths (EWs) for 4643 absorption lines. The EWs are generated from a synthetic grid which covers the ranges $3600 < T_{\rm eff} < 7400$ K, $0.2 <$ log $g < 5.4$, and $-2.4 <$ [M/H] < 0.4. Each spectrum in the synthetic grid was synthesized by `MOOG` (Sneden 1973), after adopting the ALTAS9 model atmospheres (Castelli & Kurucz 2003). Based on input trial values of $T_{\rm eff}$, log g, and [elements/H], `SP_Ace` calculated the expected EWs by interpolation using the library to generate a normalized model spectrum. Then, using the Levenberg-Marquadt method, it attempts to minimize the χ^2 between the model and the observed spectrum to determine the stellar parameters and chemical abundances. As the lines used to measure the abundances of the individual elements and stellar parameters in `SP_Ace` are well described in Boeche & Grebel (2016), we refer the interested reader to their paper.

Even though we obtained spectra of both the blue and red channels with the DIS instrument, we exclusively used the red channel spectra, because the adopted wavelength ranges (5212 – 6860 Å and 8400 – 8920 Å) used by `SP_Ace` cover a much larger wavelength range in the red. We applied `SP_Ace` to the spectra of the co-added spectra of our program stars as well as to the spectra of individual exposures of the reference stars to derive final estimates of the stellar parameters and chemical abundances.

Before we finalized the stellar parameters and chemical abundances of our program stars for the analysis of the abundance patterns, we first compared our derived values with the values for the standard stars from the various references, as a function of S/N, in order to check for systematic offsets and estimate the precision of the derived stellar parameters and chemical abundances. Table 2 lists the adopted stellar parameters and chemical abundances of the comparison stars from various references.

Figure 3 shows the differences between our values and the reference values for $T_{\rm eff}$, log g, and [Fe/H], as a function of S/N, for the standard stars. The blue star symbol with an error bar indicates the median value and median absolute deviation (MAD), respectively, in each S/N bin. We considered four bins ($<$ 50, 50 – 100, 100 – 150, and $>$ 150), separated by the vertical dotted lines in the figure. For $T_{\rm eff}$ and log g, we do not notice any significant trend with S/N. In the case of the metallicity, our derived value increases with decreasing S/N, as expected. As the typical S/N of the spectra of our program stars is less than 50, we checked the systematic offset of each parameter in the range of S/N $<$ 50. We found a median offset of $T_{\rm eff} = 99 \pm 183$ K, log $g = -0.16 \pm 0.34$ dex, and [Fe/H] $= -0.04 \pm 0.09$ dex, respectively, in the sense that our values are higher for $T_{\rm eff}$ and lower for log g and [Fe/H]. The uncertainty is the MAD. We decided to adjust the parameter scales by these offsets for derivation of the final estimates for our program stars.

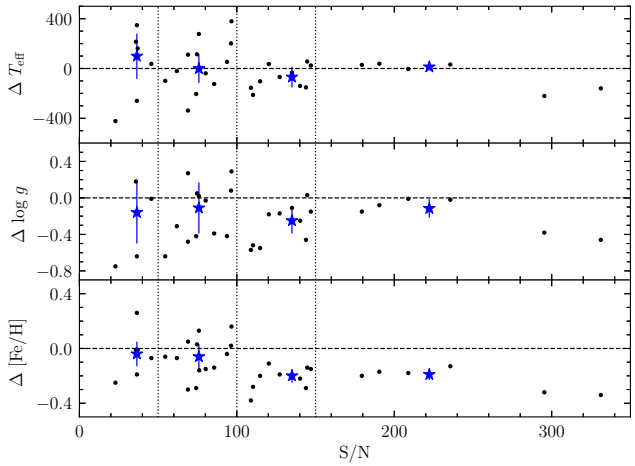

Figure 3. Differences (residuals) between estimated values and reference values for three stellar parameters of our comparison stars, as a function of S/N. The blue star symbol with an error bar indicates the median value and its median absolute deviation (MAD) calculated in each S/N range. There are four S/N ranges shown (< 50, 50 – 100, 100 – 150, and > 150), separated by the vertical dotted lines.

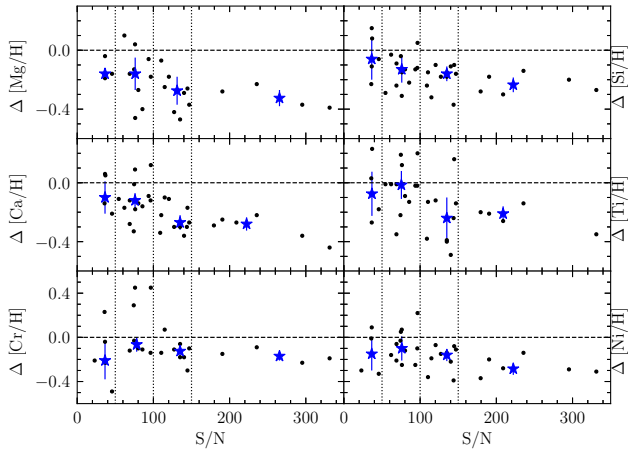

Figure 4. Same as in Figure 3, but for the chemical abundances of Mg, Si, Ca, Ti, Cr, and Ni. Note that the lower number of points for S/N < 50 results from a lower number of abundance measurements, due to absorption features being too weak.

We carried out a similar exercise for the chemical abundances (Mg, Si, Ca, Ti, Cr, and Ni); Figure 4 displays the results. Similar to [Fe/H], there is a tendency toward deriving larger abundances with decreasing S/N. For S/N < 50, we found median offsets of [Mg/H] = –0.16 ± 0.03 dex, [Si/H] = –0.06 ± 0.14 dex, [Ca/H] = –0.10 ± 0.11 dex, [Ti/H] = –0.08 ± 0.15 dex, [Cr/H] = –0.21 ± 0.17 dex, and [Ni/H] = –0.15 ± 0.15 dex. The uncertainty is the MAD. We applied these offsets to our program stars. Table 3 lists the offset-corrected stellar parameters and chemical abundances for our program stars. The value of [α/Fe] is a mean of the four ratios [Mg/Fe], [Si/Fe], [Ca/Fe], and [Ti/Fe]. The typical errors on the abundances for our target stars are σ[Mg/Fe] = 0.27 dex, σ[Si/Fe] = 0.17 dex, σ[Ca/Fe] = 0.15 dex, σ[Ti/Fe] = 0.18 dex, σ[Cr/Fe] = 0.20 dex, and σ[Ni/Fe] = 0.18 dex. These uncertainties and the uncertainties on $T_{\rm eff}$, log g, and [Fe/H] are calculated by adding in quadrature the internal error from `SP_Ace` and the MAD in the range of S/N < 50 for the standard stars. We use these corrected values for the analysis of chemical properties throughout this paper.

As setting S/N values to different limits in Figures 3 and 4 can result in different offsets in each parameter and abundance, we carried out an exercise to evaluate its effect by applying different limits of S/N, for example bins of S/N < 50, S/N = 50 – 90, S/N = 90 – 150, and S/N > 150. We did not find any significant difference from our original S/N limits, but the offsets all agreed within the errors. In particular, the differences in the chemical abundances from various different S/N limits are less than 0.02 dex, implying that S/N effect do not affect the interpretation of the chemical properties of our program stars. The reason for the small offsets among the different S/N bins is that we take a median value of the data points in each SNR bin.

Also note that the reason for the smaller offset at the low S/N in Figures 3 and 4 is that, as the noise in a low S/N spectrum can mimic extra absorption, the estimated abundance tends to be larger. We generally see this tendency in Figures 3 and 4 for our standard stars. For this reason, we adjusted the stellar parameters and chemical abundances of our programs by the offsets derived from S/N < 50.

4. KINEMATIC AND CHEMICAL PROPERTIES OF OUR PROGRAM STARS

4.1. Kinematic Properties

The contradicting results for the SEGUE low-mass candidate HVSs between Pal14 and Ziegerer et al. (2015) stem from the proper motions that they adopted. Pal14 used the SDSS proper motions (Munn et al. 2004, 2008), while Ziegerer et al. (2015) derived the proper motions from images from SDSS, DSS, and UKIDSS. Table 4 summarizes these different sets of proper motions for our target stars, along with those reported in the *Gaia* DR2.

Comparison of the three sets of proper motions reveals that the proper motions adopted by Pal14 are consistently larger than the other two; the proper motions of the four stars that Ziegerer et al. (2015) rederived are closer to the *Gaia* proper motions. Munn (priv. comm.) notes that the reported proper motions from Pal14, based on SDSS data, are almost certainly the result of mis-identification of the targets with other nearby stars. The SDSS proper motions of the other two stars (Pal14 IDs 7 and 10) that Ziegerer et al. (2015) could not measure the proper motions for are also larger than those from the *Gaia* DR2. These smaller proper motions imply that our objects are probably bound to the MW. One program star, Pal14 ID 4, exhibits a larger proper motion than the other program stars, and deserves further investigation.

Table 4
Proper motions of our program stars from different catalogs

SDSS ID	Pal14 ID	SDSS		Ziegerer et al. (2015)		*Gaia* DR2	
		$\mu_\alpha \cos\delta$ (mas yr^{-1})	μ_δ (mas yr^{-1})	$\mu_\alpha \cos\delta$ (mas yr^{-1})	μ_δ (mas yr^{-1})	$\mu_\alpha \cos\delta$ (mas yr^{-1})	μ_δ (mas yr^{-1})
J113102.87+665751.1	4	–117.2 ± 5.9	206.8 ± 5.9	–12.9 ± 2.4	–20.0 ± 4.1	–18.01 ± 0.07	–26.86 ± 0.07
J064337.13+291410.0	7	–23.6 ± 2.6	29.9 ± 2.6	···	···	0.35 ± 0.38	–2.43 ± 0.33
J172630.60+075544.0	10	19.7 ± 2.9	–56.4 ± 2.9	···	···	–6.21 ± 0.51	1.56 ± 0.48
J095816.39+005224.4	15	–58.6 ± 5.4	8.1 ± 5.4	1.1 ± 2.2	–2.2 ± 2.3	–4.20 ± 0.57	–1.27 ± 0.85
J074728.84+185520.4	16	0.8 ± 5.7	–58.1 ± 5.7	–5.2 ± 4.6	1.1 ± 5.1	–3.07 ± 0.29	–0.91 ± 0.24
J064257.02+371604.2	17	25.2 ± 2.5	42.1 ± 2.5	12.5 ± 3.2	13.0 ± 3.5	1.40 ± 0.20	–2.74 ± 0.19

Table 5
Velocities and orbital parameters of our program stars

SDSS ID	Pal14 ID	v_r (km s^{-1})	d (kpc)	U (km s^{-1})	V (km s^{-1})	W (km s^{-1})	r_{min} (kpc)	r_{max} (kpc)	Z_{max} (kpc)	e	V_{GRF} (km s^{-1})
J113102.87+665751.1	4	–65.4±3.2	1.14	24.6±13.1	–179.9±30.2	14.1±11.5	0.90±0.65	8.71±0.20	1.04±0.26	0.83±0.12	49.1±17.8
J064337.13+291410.0	7	9.6±3.4	3.16	–2.2±3.6	–32.1±8.5	–1.7±5.4	8.56±0.46	11.11±0.64	0.65±0.14	0.13±0.04	187.9±8.4
J172630.60+075544.0	10	–37.6±3.9	3.35	42.0±6.8	–51.1±9.5	84.4±19.6	3.77±0.54	7.02±0.21	2.53±0.57	0.41±0.07	193.4±7.9
J095816.39+005224.4	15	3.2±3.4	2.19	18.9±8.4	–13.8±7.4	–23.7±8.3	8.36±0.49	9.52±0.34	1.67±0.39	0.06±0.03	208.4±6.7
J074728.84+185520.4	16	35.5±3.0	3.71	41.3±5.2	–9.8±3.7	–33.2±9.9	10.77±0.71	12.70±1.20	2.05±0.67	0.06±0.02	216.7±4.6
J064257.02+371604.2	17	–1.7±3.2	1.88	–11.3±2.9	–23.4±6.3	8.1±1.8	8.20±0.18	9.83±0.37	0.56±0.11	0.10±0.03	197.1±6.2

Here, v_r is the radial velocity. U, V, and W velocities were calculated assuming V_{LSR} = 220 km s^{-1} and (–10.1, 4.0, 6.7) km s^{-1} of solar peculiar motion (Hogg et al. 2005). V_{GRF} is the Galactic rest-frame velocity.

We computed space velocity components and orbital parameters, as listed in Table 5, using radial velocities measured from the obtained spectra, proper motions from the *Gaia* DR2, and distances estimated by the SEGUE Stellar Parameter Pipeline (SSPP; Allende Prieto et al. 2008; Lee et al. 2008a,b), based on the methodology of Beers et al. (2000, 2012). The quoted distance uncertainty is on the order of 15–20%. Because the *Gaia* DR2 does not provide parallax measurements for two of our program stars, we adopted photometric distances from the SSPP, even though the distance uncertainties of four program stars derived by *Gaia* DR2 are much smaller (around 10%). We compared photometric distances and *Gaia* DR2 parallaxes for those four stars and confirmed that our photometric distances agreed with the *Gaia* distances within the error ranges.

The U, V, and W velocity components were calculated assuming 220 km s^{-1} as the rotation velocity of the local standard of rest (LSR) and $(U_\odot, V_\odot, W_\odot) = (-10.1, 4.0, 6.7)$ km s^{-1} as the solar peculiar motion (Hogg et al. 2005). Velocity components are positive in the radially outward direction from the Galactic center for U, the direction of solar rotation for V, and the direction of the North Galactic Pole for W.

The orbital parameters for individual objects were computed using the Galactic gravitational potential `MWPotential2014` (Bovy 2015), which is composed of a bulge with a power-law density, a disk parameterized by a Miyamoto-Nagai potential with mass $6.8 \times 10^{10}\ M_\odot$, and a dark-matter Navarro-Frenk-White halo potential. The distance of the Sun from the Galactic center is set to $R_\odot = 8.0$ kpc. We derived the minimum (r_{min}) and maximum (r_{max}) distances from the Galactic center, and the maximum distance (Z_{max}) from the Galactic plane during the orbit of a given star. Additionally, the eccentricity (e) was obtained from $e = (r_{max} - r_{min})/(r_{max} + r_{min})$. Table 5 lists the calculated velocity components and the derived orbital parameters. The error on each velocity and orbital parameter in the table was estimated from the standard deviation of the distribution of a sample of stars randomly re-sampled 100 times, assuming a normal error distribution for the distance, radial velocity, and proper motion.

Figure 5 is a Toomre diagram for our program stars, which can be used to kinematically classify different Galactic stellar components. In the figure, the blue and red squares represent the velocities computed with the proper motions from SDSS and *Gaia* DR2, respectively. Black and red circles roughly delineate the boundaries of the thin and thick disks, at constant velocities of 70 km s^{-1} and 180 km s^{-1} (Venn et al. 2004), respectively. The local Galactic escape speed of $V_{esc} = 533$ km s^{-1} (Piffl et al. 2014) is plotted as a blue circle. The figure clearly indicates that our spectroscopically-observed HVS candidates are all bound to the MW when the *Gaia* DR2 proper motions are used. According to this diagram, kinematically, two of our stars appear to belong to the thick disk, while four of them are likely members of the thin disk.

The separation of Galactic components is checked as follows. With the space velocity components (U, V, W) of our program stars in hand, we performed a test to compute the likelihood of belonging to the thin disk, thick disk, and the halo, following the methodology of Bensby et al. (2003). Assuming stellar populations in the thin disk, thick disk, or the halo, respectively, with Gaussian velocity distributions with different space velocities (U, V, W) and asymmetric drifts, we attempt to

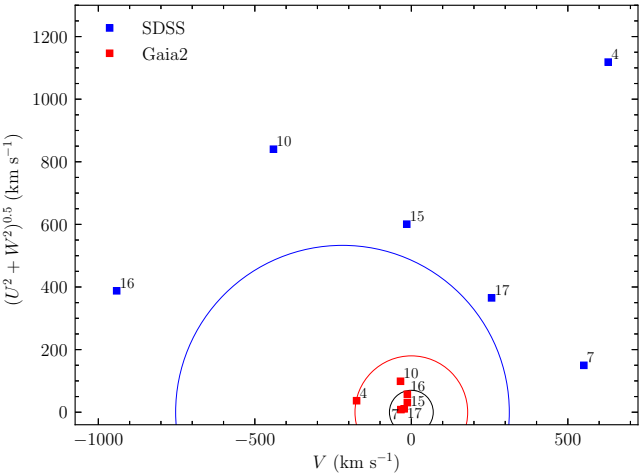

Figure 5. Toomre diagram for our sample of stars. The blue symbols indicate the velocities calculated with the SDSS proper motions, while the red symbols are based on the *Gaia* DR2 proper motions. The black and red circles roughly represent the kinematic boundaries of the thin and thick disks, at a constant velocity of 70 km s^{-1} and 180 km s^{-1} (Venn et al. 2004), respectively. The blue line indicates the local Galactic escape speed of $V_{\rm esc}$ = 533 km s^{-1} (Piffl et al. 2014). The numbers besides each star are the sample ID used by Pal14.

separate our HVS candidates into the thin disk, thick disk, or halo component by calculating the probability of belonging to one of these components. In that process, we adopted the local stellar densities, velocity dispersions in U, V, and W, and the asymmetric drifts listed in Table 1 of Bensby et al. (2003).

For each star, we compared the probabilities of being a member of any of the stellar components and assigned the star to the component with the higher likelihood. For example, if a star has a higher likelihood of being part of the thick disk relative to being part the thin disk, that is Pr(Thick)/Pr(Thin) > 5, this star is assigned to the thick disk. On the other hand, the thin disk is assigned when a star has Pr(Thick)/Pr(Thin) < 0.5. Our test revealed that only Pal14 IDs 4 and 10 have Pr(Thick)/Pr(Thin) much larger than 5, and the rest of the stars have less than 0.05. The probability of being in the halo population is much lower, Pr(Halo)/Pr(Thick) < 0.01. Only one star, ID 4, has Pr(Halo)/Pr(Thick) ∼ 0.9, which is still too small to be identified as a halo star. Thus, we conclude that each of our program stars belongs either to the thin or to the thick disk.

We also compared the Galactic rest-frame velocity ($V_{\rm GRF}$) for each star with the local escape velocity to check if it is bound to the MW. A total of one million Monte Carlo realizations were carried out to calculate the Galactic rest-frame velocities after randomly re-sampling from a normal error distribution of the radial velocities, distances, and proper motions from *Gaia* DR2. The probability of being bound is defined by the fraction of the stars that exceed the local escape velocity to the total number of stars in the simulation. We found that all our samples are, as expected, bound to the MW.

To investigate the orbital characteristics of our program stars, we integrated the orbit of each star over 2 Gyr from its current position. Figure 6 shows the orbital trajectories of our program stars projected into the Z–R (left panels) and X–Y planes (right panels). Z is the distance from the Galactic plane, R is the distance from the Galactic center projected onto the Galactic plane. X and Y are based on the Cartesian reference system in which the center of the Galaxy is at the location at (0, 0) kpc, and the Sun is located at (X, Z)=(8.0, 0.0) kpc. The filled circle indicates the current location of each star. In this figure, we clearly see that four objects (Pal14 IDs 7, 15, 16, and 17) spend most of their time outside the solar circle (upper-left panel) on nearly circular orbits (upper-right panel), with eccentricities $e < 0.15$. Judging from the orbits and U, V, W velocities, Pal14 ID 7 and 17 are typical thin-disk stars, as they are confined to $|Z| < 0.7$ kpc, while Pal14 ID 15 and 16 appear to belong to the thick disk, as they exhibit excursions above $|Z| > 1.5$ kpc.

The bottom panels of Figure 6 indicate that the other two stars in our sample (Pal14 IDs 4 and 10) are mostly inside the solar radius (lower-left panel) moving on highly eccentric orbits (lower right) with $e = 0.83$ for Pal14 ID 4 and $e = 0.41$ for Pal14 ID 10. Even though Pal14 ID 4 exhibits thick-disk kinematics, an external origin from a disrupted dwarf galaxy cannot be ruled out for this object given its high eccentricity.

4.2. Chemical Properties

Even though the kinematics provide valuable information on which Galactic component a given star is likely to be a member of, the orbits of disk stars can change over the course of several Gyr due to perturbations by transient spiral patterns or giant molecular clouds. However, since the abundance of a chemical element is essentially constant over the main sequence lifetime of a dwarf star, it can provide additional information on its likely parent Galactic component.

The α-elements such as Mg, Si, Ca, and Ti, are good indicators of the star-formation history (duration and intensity) of a stellar population (Tinsley 1979). These elements are produced by successive capture of α-particles in massive stars, which explode as core-collapse supernova (CCSN) that enrich the surrounding interstellar medium (ISM) with these elements. Early on, the ISM of a stellar population is enriched by CCSNs, and later by Type Ia SNe which produce more iron-peak elements. Consequently, high abundances of α-elements relative to Fe in a stellar population indicate that it experienced rapid star formation, while relatively low abundances suggest slow, prolonged star formation.

Figure 7 exhibits the abundances of Mg, Si, Ca, Ti, Cr, and Ni relative to Fe as a function of [Fe/H], for five different Galactic stellar populations – thin disk (red circles), thick disk (filled blue circles), bulge (green

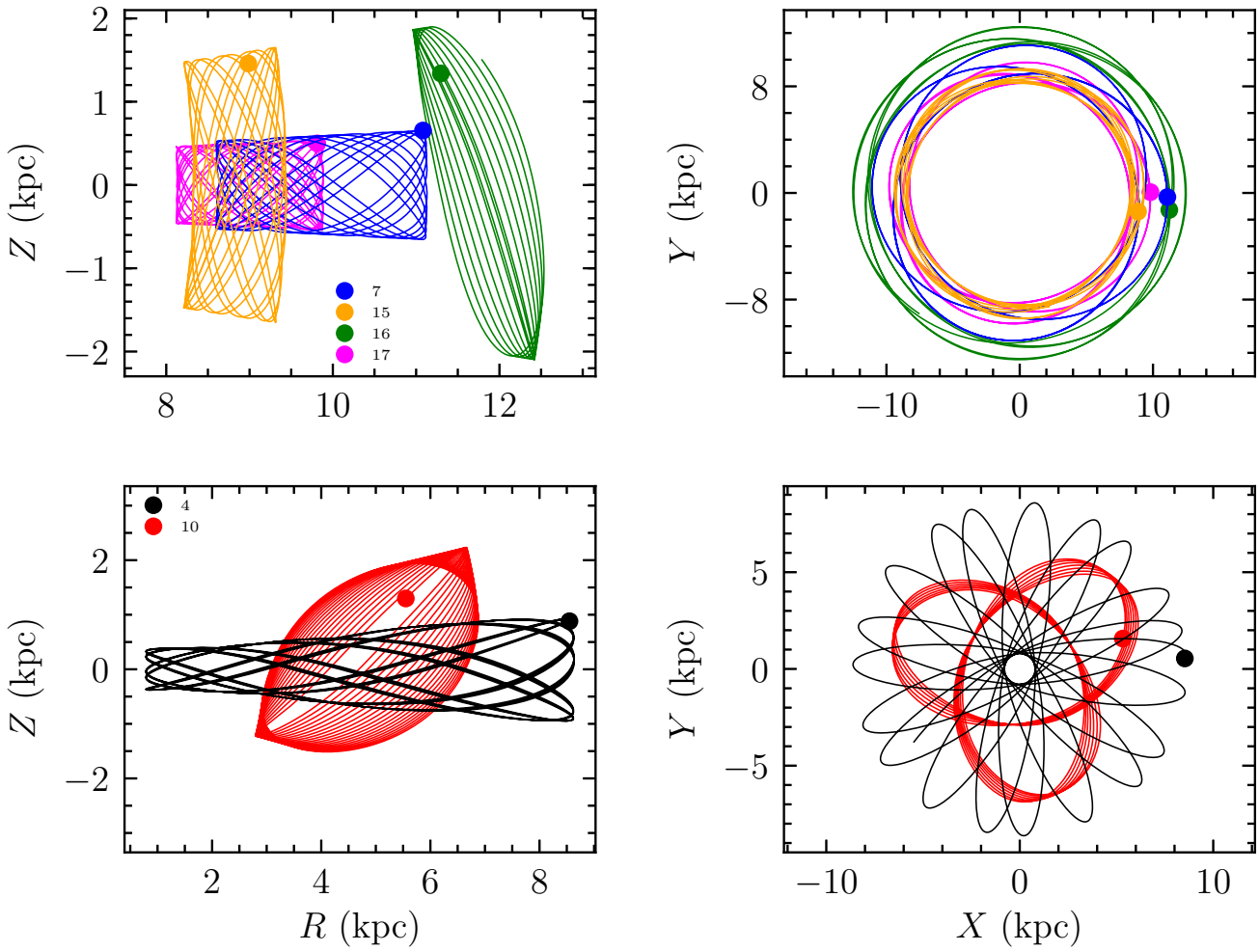

Figure 6. Projected orbits for our program stars over 2 Gyr from the present, in the planes spanned by Z and R (left panels) and X and Y (right panels), respectively. Z is the distance from the Galactic plane, while R is the distance from the Galactic center projected onto the Galactic plane. X and Y are based on the Cartesian reference system, in which the center of the Galaxy is located at (0, 0) kpc and the Sun is located at $(X, Z) = (8.0, 0.0)$ kpc. A filled circle indicates the current location of a star.

triangle), halo (filled orange square), and LMC stars (black circles). Our program stars are represented by star symbols. Chemical abundances for bulge stars are from Alves-Brito et al. (2010); Johnson et al. (2014), for halo stars from Alves-Brito et al. (2010); Reddy et al. (2006), for thin and thick disk stars from Alves-Brito et al. (2010); Bensby et al. (2003); Reddy et al. (2006), and for LMC stars from Van der Swaelmen et al. (2013).

From inspection of Figure 7, general trends for each population are the following. The thick-disk and halo stars exhibit similar trends, as they are rich in α-elements, but relatively low in Cr and Ni. The thick-disk stars are more metal-rich ([Fe/H] $>$ –0.9) than the halo stars ([Fe/H] $<$ –0.8). The bulge stars display a wide range of metallicity, showing an enhancement of α-elements that leads to overlap with the thick disk. Their α-abundances decrease with increasing metallicity and eventually connect to the distribution for the thin disk. However, the Ca abundances (partially Ni as well) of the bulge stars are consistently higher than the ones of thick- and thin-disk populations. Therefore, the Ca abundance plays a key role in distinguishing bulge stars from disk stars. The LMC stars exhibit abundances for Mg, Si, Ca, and Ni elements that are systematically lower than the ones of the other Galactic components, but overlap with other Galactic stars in Ti and Cr. We included the LMC stars into our comparison because there is a possibility that runaway stars may come from the LMC (Boubert & Evans 2016). We also note that there is no clear distinction among the Galactic components in the Fe-peak element Cr. The Ni abundance of bulge stars in the range –0.5 $<$ [Fe/H] $<$ 0.2 is higher than the one for than any other Galactic population. Our program stars, indicated with star symbols, all have metallicity larger than [Fe/H] = –0.7; none of them is likely to be a halo star.

While some of our program stars overlap with one or two Galactic stellar populations in their chemical

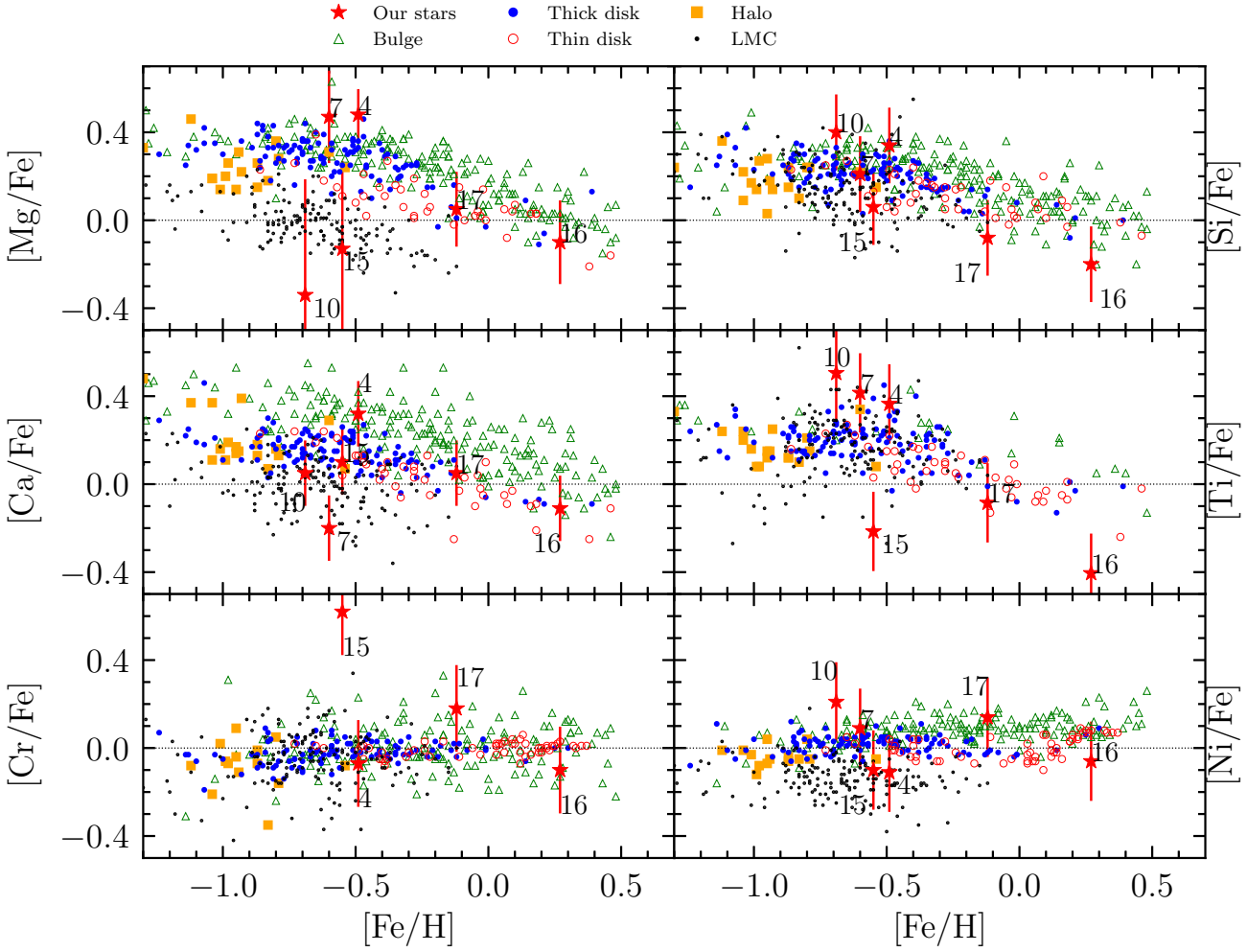

Figure 7. Abundance ratios of Mg, Si, Ca, Ti, Cr, and Ni, as a function of [Fe/H], for stars in the Galactic bulge (green triangles; Alves-Brito et al. 2010; Johnson et al. 2014), the thick disk (filled blue circles; Alves-Brito et al. 2010; Bensby et al. 2003; Reddy et al. 2006), the thin disk (red circles; Alves-Brito et al. 2010; Bensby et al. 2003; Reddy et al. 2006), the halo (filled orange squares; Alves-Brito et al. 2010; Reddy et al. 2006), and the LMC (black dots; Van der Swaelmen et al. 2013). Our program stars are displayed as red star symbols along their Pal14 IDs.

characteristics, most of our stars exhibit element abundances that somewhat deviate from the comparison stellar populations. The star Pal14 ID 16, which is the most-Fe rich object in our sample, appears to belong to the thin disk, because the Mg, Si, Ca, and Cr abundances agree with those of the thin-disk stars, although the Ti and Ni abundances are lower than the ones of other thin-disk stars. It is also consistent with the chemistry of the bulge population. Pal 14 ID 17 is likely to be associated with the thin disk as the abundances of most elements are similar to the ones of thin-disk stars, considering the error bars on Cr and Ni. Pal14 ID 4 is likely to be a bulge star because of the enhancement of all of its α-elements. Pal14 ID 15 appears to be a metal-poor thin-disk star as its α-element abundances are lower than the ones for the thick disk, although the Cr abundance stands out with respect to the other elements. Pal14 ID 7 may be a thick-disk star, because its Mg, Si, and Ti are enhanced and the Ca abundance does not point to the bulge component, but rather the LMC. Taking into account the large error bar for Mg, Pal14 ID 10 appears to belong to the thick disk, with enhanced Si and Ti.

5. DISCUSSION

Even though our HVS stars turned out to be disk stars based on the kinematic probabilistic membership assignment as described in Section 4.1, some of them have dynamical properties distinct from canonical disk stars as discussed below. In the following, we consider a star with high eccentricity to be either an accreted or heated disk star because stars from a disrupted dwarf galaxy are expected to exhibit high eccentricities, as do dynamically heated stars. We regard stars with low eccentricity but comparatively large excursions from the Galactic plane to be possible runaway stars.

Table 6
Possible origins of our program stars

SDSS ID	Pal14 ID	Galactic component	Possible origin(s)
J113102.87+665751.1	4	Bulge	Accreted or heated
J064337.13+291410.0	7	Thick	···
J172630.60+075544.0	10	Thick	Runaway or heated
J095816.39+005224.4	15	Thin	Runaway
J074728.84+185520.4	16	Thin	Runaway
J064257.02+371604.2	17	Thin	···

5.1. SDSS J113102.87+665751.1 (Pal14 ID 4)

As this star has [Fe/H] = –0.49, and a high value of [α/Fe] = 0.38, one might consider this object to be a typical thick-disk star. However, several α-elements appear to be enhanced with respect to the thick-disk population and to be closer to the bulge population, especially Ca which is the key element to distinguish between thick-disk and bulge stars. Thus, it is reasonable to infer that it is a bulge star.

The calculated orbital parameters for this star are $Z_{\rm max}$ = 1.04 kpc, e = 0.83, $r_{\rm min}$ = 0.90 kpc, and $r_{\rm max}$ = 8.71 kpc; hence its orbit spans from the near bulge through the solar radius with a very high eccentricity. Note that our $r_{\rm min}$ value is rather smaller than that of Ziegerer et al. (2015) due to the slightly larger proper motions from *Gaia* DR2. These chemical and dynamical characteristics suggest that this star was born in the bulge and reached its current location through mechanisms such as dynamical ejection in a high stellar density environment or binary supernova ejection. However, its Galactic rest-frame velocity of $V_{\rm GRF}$ = 49.1 km s^{-1} is too small to consider that origin likely. Rather, its orbit points to it being a former member of a disrupted dwarf galaxy or a dynamically heated disk star.

5.2. SDSS J064337.13+291410.0 (Pal14 ID 7)

This star has [Fe/H] = –0.60 and [α/Fe] = 0.22, typical for a thick-disk star. Looking into the individual α-elements, the Mg and Ti abundances are higher and the Ca abundance is lower than that of most stars in the thick-disk population. Only the Si and Ni abundances are close to those of other thick-disk stars.

The kinematics also suggests that this object is a thick-disk star, with orbital parameters $Z_{\rm max}$ = 0.65 kpc, e = 0.13, $r_{\rm min}$ = 8.56 kpc, and $r_{\rm max}$ = 11.11 kpc. Combining the chemical and kinematic characteristics, this star may be born in the outer disk, and is now located close to the solar circle.

5.3. SDSS J172630.60+075544.0 (Pal14 ID 10)

With metallicities [Fe/H] = –0.69 and [α/Fe] = 0.15, this object can also be regarded as a thick-disk star. Yet, the abundances of four α-elements exhibit a complex pattern; the Ca abundance is in the thick disk region, whereas the Si and Ti abundances are higher than the ones for the rest of the thick-disk population. The Ni abundance is also larger than that of the thick disk. Taking into account the large uncertainty of the Mg abundance, we consider this object to be a thick-disk star.

Kinematically, however, this object has an eccentricity of e = 0.41 and $r_{\rm min}$ = 3.77 kpc, and its vertical height is as high as $Z_{\rm max}$ = 2.53 kpc. Combined with the chemical signatures, this object may be a dynamically heated disk star. It is also possible that this star may be a disk runaway star, originating from near the bulge, or a heated disk star, as it reaches a comparatively large vertical height. The high eccentricity is also consistent with a possible external origin from a dissolved dwarf galaxy, but the extent of its orbit (only exploring 2 kpc away) appears to be too small to be commensurate with accretion.

5.4. SDSS J095816.39+005224.4 (Pal14 ID 15)

The metallicities [Fe/H] = –0.55 and [α/Fe] = –0.05 for this star indicate a metal-poor thin-disk star. The chemical abundances of individual elements agree with those of the thin-disk population within the error bars, except the relatively low Ti and high Cr abundances compared to those of any Galactic population.

The orbital parameters $r_{\rm min}$ = 8.36 kpc, $Z_{\rm max}$ = 1.67 kpc, and e = 0.06 also suggest a thin-disk star. As this star reaches up to Z = 1.67 kpc, it is a good candidate for a disk runaway star ejected by a SNe explosion in a binary system. As Bromley et al. (2009) found in simulations, some runaway stars exhibit kinematics similar to disk or halo stars.

5.5. SDSS J074728.84+185520.4 (Pal ID 16)

This object has the highest metallicity in our sample, [Fe/H] = 0.27, and its [α/Fe] value is –0.20. All six elements show abundance ratios lower than the Sun, which mimic the pattern of a metal-rich thin-disk star. Hence, one may consider this star to belong to the thin disk.

Likewise, the orbital parameters $r_{\rm min}$ = 10.77 kpc, $Z_{\rm max}$ = 2.05 kpc, and e = 0.06 imply a thin-disk star. As can be seen from Figure 6, this object resides in the outer disk and undergoes large excursions, with a small eccentricity, above the Galactic plane. Thus, it is more plausible to infer that this object is a runaway star from the thin-disk population.

5.6. SDSS J064257.02+371604.2 (Pal ID 17)

Pal14 ID 17 is a metal-rich ([Fe/H] = –0.12) star with an essentially solar α ratio ([α/Fe] = –0.02). The abundances of the individual α-elements are overlapped with those of the thin-disk population, whereas the iron-peak elements appear more consistent with the bulge. Its orbital parameters ($r_{\rm min}$ = 8.20 kpc, $Z_{\rm max}$ = 0.56 kpc, and e = 0.10) also point to a typical thin-disk star.

6. SUMMARY AND CONCLUSIONS

We presented a chemodynamical analysis of six low-mass dwarf stars, alleged to be HVSs by Pal14, in order

to determine from which Galactic component they originate. Based on kinematic analysis using accurate *Gaia* DR2 proper motions, we confirm that all six objects are bound to the MW, as noted previously by Ziegerer et al. (2015). Our conclusion is also upheld by the recent study by Boubert et al. (2018), who performed a detailed investigation of late-type HVS candidates with proper motions from *Gaia* DR2, and found that almost all known late-type HVS candidates are bound to the Galaxy. The HVS status for the low-mass stars identified by Pal14 is mainly due to the incorrect assignment of proper motions.

Nonetheless, we attempted to characterize the parent Galactic stellar components and origins of our program stars by means of a comparison of their chemical abundance patterns with the ones of various Galactic stellar components, together with their orbital properties. The probabilistic assignment of membership to Galactic components based on kinematics revealed that our program stars belong to the thin or thick disk. However, since four of the six stars exhibit peculiar dynamical properties and chemical characteristics compared to canonical disk stars, we cannot rule out exotic origins such as runaway, disk heating, and accretion from dwarf galaxies as discussed, as summarized below and in Table 6.

We identify two typical disk stars (Pal14 IDs 7 and 17); Pal14 ID 7 is a typical thick disk star, while Pal ID 17 is a typical thin-disk star. Our stars show abundance patterns similar to that of stars in the Galactic thick and thin disk, respectively, and have nearly circular orbits.

One star (Pal14 ID 4) may originate from the Galactic bulge, as its orbit passes close to the bulge with a high eccentricity. Moreover, the abundances of the α-elements for this star all agree with those of other Galactic bulge stars. One may think that this star may be ejected from the bulge by dynamical ejection or SNe ejection mechanism. However, its $V_{\rm GRF}$ is too small to consider such an origin likely. Rather, its high-eccentricity orbit suggests accretion from a disrupted dwarf galaxy, or dynamical heating.

Pal14 ID 10 may be a runway or heated disk star, as it reaches as high as 2.53 kpc from the Galactic plane during its orbit, and its chemical abundance pattern is, within errors, in agreement with the thick-disk population.

Pal14 ID 15 appears to be a runaway from the Galactic disk, because it exhibits a large excursion ($Z_{\rm max} = 1.67$ kpc) from the Galactic plane and follows an almost circular ($e = 0.06$) orbit that reaches beyond the solar radius. Its chemical abundance pattern, which is similar to the one of other metal-poor thin-disk stars, supports this idea.

Finally, Pal14 ID 16, which has the highest metallicity in our sample, exhibits chemical abundances similar to a very metal-rich thin-disk star, while its orbit exhibits a large excursion ($Z_{\rm max} = 2.05$ kpc) from the Galactic plane beyond $R = 11$ kpc. We consider this star to be a runaway star from the Galactic disk.

Although all of our spectroscopically observed candidate HVSs turned out to be bound to the Galaxy, and to be not even particularly fast-moving objects, some of our program stars exhibit exotic orbits. Thus, future higher resolution spectroscopic follow-up observations for these curious stars may be of interest, and provide a better understanding of their origin.

ACKNOWLEDGMENTS

We thank the anonymous referees for their careful review of this manuscript, and for suggesting a number of improvements.

This research has made use of the VizieR catalog access tool, CDS, Strasbourg, France. This work has made use of data from the European Space Agency (ESA) mission *Gaia*[5] processed by the *Gaia* Data Processing and Analysis Consortium (DPAC). [6] Funding for the DPAC has been provided by national institutions, in particular the institutions participating in the *Gaia* Multilateral Agreement.

Funding for SDSS-III[7] was provided by the Alfred P. Sloan Foundation, the Participating Institutions, the National Science Foundation, and the U.S. Department of Energy Office of Science.

Y.S.L. acknowledges support from the National Research Foundation (NRF) of Korea (grants no. 2017R1A5A1070354 and 2018R1A2B6003961). T.C.B. acknowledges partial support from grant PHY 14-30152 by the Physics Frontier Center / JINA Center for the Evolution of the Elements (JINA-CEE) awarded by the National Science Foundation of the USA.

REFERENCES

Abadi, M. G., Navarro, J. F., & Steinmetz, M. 2009, An Alternative Origin for Hypervelocity Stars, ApJL, 691, L63

Allende Prieto, C., Sivarani, T., Beers, T. C., et al. 2008, The SEGUE Stellar Parameter Pipeline. III. Comparison with High-Resolution Spectroscopy of SDSS/SEGUE Field Stars, AJ, 136, 2070

Alves-Brito, A., Meléndez, J., Asplund, M., et al. 2010, Chemical Similarities between Galactic Bulge and Local Thick Disk Red Giants: O, Na, Mg, Al, Si, Ca, and Ti, A&A, 513, 35

Battistini, C., & Bensby, T. 2015, The Origin and Evolution of the Odd-Z Iron-Peak Elements Sc, V, Mn, and Co in the Milky Way Stellar Disk, A&A, 577, 9

Beers, T. C., Carollo, D., Ivezić, Ž., et al. 2012, The Case for the Dual Halo of the Milky Way, ApJ, 746, 34

Beers, T. C., Chiba, M., Yoshii, Y., et al. 2000, Kinematics of Metal-poor Stars in the Galaxy. II. Proper Motions for a Large Nonkinematically Selected Sample, AJ, 119, 2866

Bensby, T., Feltzing, S., & Lundstrom, I. 2003, Elemental Abundance Trends in the Galactic Thin and Thick Disks as Traced by Nearby F and G Dwarf Stars, A&A, 410, 527

Bensby, T., Feltzing, S., & Lundstrom, I. 2005, α-, r-, and s-Process Element Trends in the Galactic Thin and Thick Disks, A&A, 433, 185

[5] https://www.cosmos.esa.int/gaia
[6] https://www.cosmos.esa.int/web/gaia/dpac/consortium
[7] http://www.sdss3.org/

Blaauw, A. 1961, On the Origin of the O- and B-Type Stars with High Velocities (the "Run-Away" Stars), and Some Related Problems, BAN, 15, 265

Boeche, C., & Grebel, E. K. 2016, SP_Ace: a New Code to Derive Stellar Parameters and Elemental Abundances, A&A, 587, 2

Boeche, C., Siebert, A., Williams, M., et al. 2011, The RAVE Catalog of Stellar Elemental Abundances: First Data Release, AJ, 142, 193

Boubert, D., & Evans, N. W. 2016, A Dipole on the Sky: Predictions for Hypervelocity Stars from the Large Magellanic Cloud, ApJL, 825, L6

Boubert, D., Guillochon, J., Hawkins, K., et al. 2018, Revisiting Hypervelocity Stars after Gaia DR2, MNRAS, 479, 2789.

Bovy, J. 2015, galpy: A Python Library for Galactic Dynamics, ApJs, 216, 29

Bromley, B. C., Kenyon, S. J., Brown, W. R., & Geller, M. J. 2009, Runaway Stars, Hypervelocity Stars, and Radial Velocity Surveys, ApJ, 706, 925

Brown, W. R. 2015, Hypervelocity Stars, ARA&A, 53, 15

Brown, W. R., Anderson, J., Gnedin, O. Y., et al. 2015, Proper Motions and Trajectories for 16 Extreme Runaway and Hypervelocity Stars, ApJ, 804, 49

Brown, W. R., Geller, M. J., & Kenyon, S. J. 2014, MMT Hypervelocity Star Survey. III. The Complete Survey, ApJ, 787, 89

Brown, W. R., Geller, M. J., Kenyon, S. J., & Kurtz, M. J. 2005, Discovery of an Unbound Hypervelocity Star in the Milky Way Halo, ApJ, 622, L33

Castelli, F., & Kurucz, R. L. 2003, Modelling of Stellar Atmospheres, ed. N. Piskunov, W.W. Weiss, and D.F. Gray (Published on behalf of the IAU by the ASP, 20)

Cenarro, A. J., Peletier, R. F., Sanchez-Blazquez, P., et al. 2007, Medium-Resolution Isaac Newton Telescope Library of Empirical Spectra – II. The Stellar Atmospheric Parameters, MNRAS, 374, 664

Cui, X.-Q., Zhao, Y.-H., Chu, Y.-Q., et al. 2012, The Large Sky Area Multi-Object Fiber Spectroscopic Telescope (LAMOST), Res. Astron. Astrophys., 12, 1197

Delgado Mena, E. G., Israelian, J. I., Gonzalez Hernandez, S. G., et al. 2014, Li Depletion in Solar Analogues with Exoplanets. Extending the Sample, A&A, 562, 92

Freeman, K., & Bland-Hawthorn, J. 2002, The New Galaxy: Signatures of Its Formation, ARA&A, 40, 487

Fulbright, J. P. 2000, Abundances and Kinematics of Field Halo and Disk Stars. I. Observational Data and Abundance Analysis, AJ, 120, 1841

Gaia Collaboration, Brown, A. G. A., Vallenari, A., et al. 2018, Gaia Data Release 2. Summary of the Contents and Survey Properties, A&A, 616, A1.

Gies, D. R. 1987, The Kinematical and Binary Properties of Association and Field O Stars, ApJS, 64, 545

Hawkins, K., & Wyse, R. F. G. 2018, The Fastest Travel Together: Chemical Tagging of the Fastest Stars in Gaia DR2 to the Stellar Halo, MNRAS, 481, 1028

Hills, J. G. 1988, Hyper-Velocity and Tidal Stars from Binaries Disrupted by a Massive Galactic Black Hole, Nature, 331, 687

Hogg, D. W., Blanton, M. R., Roweis, S. T., et al. 2005, Modeling Complete Distributions with Incomplete Observations: The Velocity Ellipsoid from Hipparcos Data, ApJ, 629, 268

Houk, N., & Swift, C. 2000, VizieR Online Data Catalog: Michigan Catalogue of HD stars, Vol. 5 (Houk+, 1999), VizieR Online Data Catalog, 3214

Johnson, C. I., Rich, R. M., Kobayashi, C., Kunder, A., & Koch, A. 2014, Light, Alpha, and Fe-peak Element Abundances in the Galactic Bulge, AJ, 148, 67

Kollmeier, J. A., & Gould, A. 2007, Where Are the Old-Population Hypervelocity Stars?, ApJ, 664, 343

Kollmeier, J. A., Gould, A., Knapp, G., & Beers, T. C. 2009, Old-Population Hypervelocity Stars from the Galactic Center: Limits from the Sloan Digital Sky Survey, ApJ, 697, 1543

Kurtz, M. J. & Mink, D. J. 1998, RVSAO 2.0: Digital Redshifts and Radial Velocities, PASP, 110, 934

Lawrence, A., Warren, S. J., Almaini, O., et al. 2007, The UKIRT Infrared Deep Sky Survey (UKIDSS), MNRAS, 379, 1599

Lee, Y. S., Beers, T. C., Prieto, C. A., et al. 2011, The SEGUE Stellar Parameter Pipeline. V. Estimation of Alpha-element Abundance Ratios from Low-resolution SDSS/SEGUE Stellar Spectra, AJ, 141, 90

Lee, Y. S., Beers, T. C., Sivarani, T., et al. 2008a, The SEGUE Stellar Parameter Pipeline. I. Description and Comparison of Individual Methods, AJ, 136, 2022

Lee, Y. S., Beers, T. C., Sivarani, T., et al. 2008b, The SEGUE Stellar Parameter Pipeline. II. Validation with Galactic Globular and Open Clusters, AJ, 136, 2050

Li, Y., Luo, A., Zhao, G., et al. 2012, Metal-Poor Hypervelocity Star Candidates from the Sloan Digital Sky Survey, ApJL, 744, 24

Li, Y.-B., Luo, A.-L., Zhao, G., et al. 2015, 19 Low Mass Hypervelocity Star Candidates from the First Data Release of the LAMOST Survey, Res. Astron. Astrophys., 15, 1364.

Mishenina, T. V., Pignatari, M., Korotin, S. A., Soubiran, C., et al. 2013, Abundances of Neutron-Capture Elements in Stars of the Galactic Disk Substructures, A&A, 552, 128

Munn, J. A., Monet, D. G., Levine, S. E., et al. 2004, An Improved Proper-Motion Catalog Combining USNO-B and the Sloan Digital Sky Survey, AJ, 127, 3034

Munn, J. A., Monet, D. G., Levine, S. E., et al. 2008, Erratum: "An Improved Proper-Motion Catalog Combining Usno-B and the Sloan Digital Sky Survey" (2004, AJ, 127, 3034), AJ, 136, 895

Palladino, L. E., Schlesinger, K. J., Holley-Bockelmann, K., et al. 2014, Hypervelocity Star Candidates in the SEGUE G and K Dwarf Sample, ApJ, 780, 7

Piffl, T., Scannapieco, C., Binney, J., et al. 2014, The RAVE Survey: the Galactic Escape Speed and the Mass of the Milky Way, A&A, 562, A91

Poveda, A., Ruiz, J., & Allen, C. 1967, Run-away Stars as the Result of the Gravitational Collapse of Protostellar Clusters, Boletin de los Observatorios Tonantzintla y Tacubaya, 4, 86

Prugniel, Ph., Vauglin, I., & Koleva, M. 2011, The Atmospheric Parameters and Spectral Interpolator for the MILES Stars, A&A, 531, 165

Reddy, B. E., Lambert, D. L., & Allende Prieto, C. 2006, Elemental Abundance Survey of the Galactic Thick Disc, MNRAS, 367, 1329

Sneden, C. 1973, Carbon and Nitrogen Abundances in Metal-Poor Stars, PhD thesis, Univ. Texas at Austin

Steinmetz, M., Zwitter, T., Siebert, A., et al. 2006, The

Radial Velocity Experiment (RAVE): First Data Release, AJ, 132, 1645
Stone, R. C. 1991, The Space Frequency and Origin of the Runaway O and B Stars, AJ, 102, 333
Takeda, Y., & Honda, S. 2005, Photospheric CNO Abundances of Solar-Type Stars, PASJ, 57, 65
Tauris, T. M. 2015, Maximum Speed of Hypervelocity Stars Ejected from Binaries, MNRAS, 448, 6
Tauris, T. M., Takens, R. J. 1998, Runaway Velocities of Stellar Components Originating from Disrupted Binaries via Asymmetric Supernova Explosions, A&A, 330, 1047
Tetzlaff, N., Neuhäuser, R., & Hohle, M. M. 2011, A Catalogue of Young Runaway Hipparcos Stars within 3 kpc from the Sun, MNRAS, 410, 190
Tinsley, B. M. 1979, Stellar Lifetimes and Abundance Ratios in Chemical Evolution, ApJ, 229, 1046
Van der Swaelmen, M., Hill, V., Primas, F., et al. 2013, Chemical Abundances in LMC Stellar Populations. II. The Bar Sample, A&A, 560, A44
Venn, K. A., Irwin, M., Shetrone, M. D., Tout, C. A., Hill, V., Tolstoy, E. 2004, Stellar Chemical Signatures and Hierarchical Galaxy Formation, AJ, 128, 1177
Watkins, L. L., Evans, N. W., & An, J. H. 2010, The Masses of the Milky Way and Andromeda Galaxies, MNRAS, 406, 264
Xue, X. X., Rix, H. W., Zhao, G., et al. 2008, The Milky Way's Circular Velocity Curve to 60 kpc and an Estimate of the Dark Matter Halo Mass from the Kinematics of ∼2400 SDSS Blue Horizontal-Branch Stars, ApJ, 684, 1143
Yanny, B., Rockosi, C., Newberg, H. J., et al. 2009, SEGUE: A Spectroscopic Survey of 240,000 Stars with g = 14-20, AJ, 137, 4377
York, D. G., Adelman, J., Anderson, J. E., Jr., et al. 2000, The Sloan Digital Sky Survey: Technical Summary, AJ, 120, 1579
Yu, Q., & Tremaine, S. 2003, Ejection of Hypervelocity Stars by the (Binary) Black Hole in the Galactic Center, ApJ, 599, 1129
Zhong, J., Chen, L., Liu, C., et al. 2014, The Nearest High-velocity Stars Revealed by LAMOST Data Release 1, ApJL, 789, L2
Ziegerer, E., Volkert, M., Heber, U., et al. 2015, Candidate Hypervelocity Stars of Spectral Type G and K Revisited, A&A, 576, 14